Monte Carlo study of the escape of a minor species

A. R. Barakat* and J. Lemaire
Institut d'Aeronomie Spatiale de Belgique, 3 Avenue Circulaire, B-1180 Brussels, Belgium
(Received 20 September 1989; revised manuscript received 19 April 1990)

The understanding of some important space-physics problems (e.g., the Jeans escape of light atoms from a planetary atmosphere and the ion escape in the terrestrial polar wind) is related to the problem of the escape of a minor species through a nonuniform background. This latter problem was studied for different interparticle collision models (Maxwell molecule and hard sphere), for different minor-to major-species mass ratios, and for different values of the escape velocity (v_c). The gravitational force was simulated by a critical escape velocity (v_c), and the Lorentz forces were ignored. First, a simple variable change was used to transform the problem into a simpler one where the background medium is uniform. This simplified problem, which is similar to the "Milne" problem, was solved by a Monte Carlo simulation. In the collisionless region and for the case of zero escape velocity ($v_c=0$), the velocity distribution function of the minor species (f_t) showed large deviations from a Maxwellian, with large temperature anisotropy (parallel temperature less than the perpendicular temperature) and asymmetry in the parallel direction (upward tail), for both of the collision models. In the collision-dominated region the normalized density gradient was found to be independent of the mass ratio for the Maxwell molecule collision. For the hard-sphere cross section, it was reduced by a mass-ratio-dependent factor. This is due to the heat-flow contribution to the momentum balance, which vanishes only for the former collision model. The Monte Carlo results were compared with the moment-equations approach and the direct solution of the Boltzmann equation. This comparison confirms that the Monte Carlo method is a viable alternative and complementary to other techniques, especially in recent years, due to the large increase in the available computation power.

I. INTRODUCTION

The problem of the escape of a minor species through a major one has a wide range of applications in many physical problems. In the field of atmospheric physics, it was applied in order to study the escape of hydrogen and helium from the terrestrial atmosphere through a background of oxygen.[1] With regard to neutron transport, the minor species is neutron gas diffusing through a moderator in a reactor.[2]

The distribution function f_t of the minor species or test particles (t) diffusing in an excess background species (b) is given by Boltzmann's equation,[3]

$$\frac{\partial f_t}{\partial t}+\mathbf{v}_t\cdot\nabla f_t+\left[\mathbf{G}+\frac{e_t}{m_t}\left[\mathbf{E}+\frac{1}{c}\mathbf{v}_t\times\mathbf{B}\right]\right]\cdot\nabla_{v_t}f_t = \int d\mathbf{v}_b\, d\Omega\, g_{tb}\sigma_{tb}(g_{tb},\chi)(f_t'f_b'-f_tf_b)\ . \tag{1}$$

In Eq. (1) $\mathbf{v}$ is the velocity, $\mathbf{G}$ is the gravitational acceleration, $\mathbf{E}$ and $\mathbf{B}$ are the electric and magnetic fields, $\mathbf{g}_{tb}$ ($=\mathbf{v}_t-\mathbf{v}_b$) is the relative velocity, Ω [$=(\phi,\chi)$] is the solid angle, σ_{tb} is the differential scattering cross section, and χ is the scattering angle. The function f_b is taken to be a Maxwellian. The primes denote quantities evaluated after collisions.

For practical problems the solution of Eq. (1) is difficult. Therefore, many physical models and mathematical techniques were developed to tackle this task, such as hydrodynamic models,[4,5] generalized transport models,[6–8] and exospheric (collisionless) models.[9–13] Each of these models is based on implicit assumptions which limit its domain of application. For instance, the hydrodynamic approximations are valid only in collision-dominated regimes, while the exospheric models (i.e., zeroth-order kinetic models) are valid when the collision term can be neglected. In the transition region between the collision-dominated and collisionless regions another method should be used.[14–16] The Monte Carlo method can be a valuable tool in this regard.

Lindenfeld and Shizgal[17] (referred to as LS hereafter) studied the Milne problem by solving directly the Boltzmann equation via expanding f_t into a series of Burnett's functions. More recently, a discrete ordinate method [now called the quadrature discretization method (QDM)] was used by Shizgal and Blackmore[1] (referred to as SB hereafter) to solve the Boltzmann equation for the problem of escape of hydrogen and helium from the Earth, as well as the escape of hydrogen from Mars. This method, which is based on the Gaussian quadrature approach has successfully been used to solve integro-differential equations.[18] Although very promising, however, major efforts are required to adapt these method to new physical conditions. Also, they require elaborate mathematical computations in comparison to the Monte Carlo method. On the other hand, Monte Carlo methods are generally more demanding with respect to central-processing-unit (CPU) time.

The Monte Carlo method is a technique that solves the Boltzmann equation by particle simulation. Its simple concept, straightforward algorithm, and its adaptability to include new features (such as electrostatic field, magnetic field, and different collision models) make it a useful tool in physics, and a powerful test of results obtained with other mathematical methods. For more than three decades, it has been used to study the diffusion of minor species through a major one.[19–23] The early attempts[19] in the 1950s were largely limited by limited computational facilities. But as computer technology improved in the following years, more computing power became available at lower expenses, and the Monte Carlo particle simulation became a more viable alternative to address physical and engineering problems.

This work has two objectives. The first is to illustrate the potential strength of Monte Carlo (MC) methods in comparison (and in combination) with the other analytical and numerical methods. This will be attempted by applying this MC method to the problem of the escape of a minor species t (test) diffusing through a dominant species b (background). As a test we compare the value of the extrapolation length and escape fluxes obtained with the different methods. The second objective is to gain a physical insight into the behavior of the minor species in the above problem. The velocity distribution function of the minor species (f_t) as well as its velocity moments (density, drift, temperature, etc.) are studied for different physical parameters.

II. FORMULATION OF THE PROBLEM

In this work we consider the steady-state escape of a minor species t through an isothermal background species b. The electromagnetic force is ignored in this first paper. The effect of the gravitational force (if any) is simulated by including a critical velocity v_c, such that a particle that leaves the upper boundary with $v > v_c$ escapes, otherwise, it is reflected downward. The background species is assumed to have a local Maxwellian distribution function, depending on the altitude z; f_b is given by

$$f_b(z,\mathbf{v}_b)=n_b(z)f_b^{(M)}(\mathbf{v}_b) , \tag{2}$$

where

$$f_b^{(M)}(\mathbf{v}_b)=\left[\frac{m_b}{2\pi kT_b}\right]^{3/2}\exp^{-(m_b v_b^2/2kT_b)} . \tag{3}$$

In Eqs. (2) and (3), n_b is the number density, $\mathbf{v}_b$ is the velocity, m_b is the mass of the particle, k is the Boltzmann constant, and T_b is the temperature of the background particles (T_b is assumed to be constant).

According to these assumptions, Eq. (1) takes the form

$$v_{t_\parallel}\frac{\partial f_t}{\partial z}=n_b(z)\int d\mathbf{v}_b\, d\Omega\, g_{tb}\sigma_{tb}(g_{tb},\chi)(f_t' f_b'^{(M)}-f_t f_b^{(M)}) . \tag{4}$$

Changing the variables, we can recast Eq. (4) in the form

$$-v_{t_\parallel}\frac{\partial f_t}{\partial \tilde{z}}=D\int d\mathbf{v}_b d\Omega\, g_{tb}\sigma_{tb}(g_{tb},\chi)(f_t' f_b'^{(M)}-f_t f_b^{(M)}) , \tag{5}$$

where

$$\tilde{z}=\int_z^\infty dz'\frac{\nu_{tb}(z')}{\sqrt{2kT_b/m_t}} , \tag{6}$$

$$D=\sqrt{2kT_b/m_t}/\nu_{tb}^* , \tag{7}$$

$$\nu_{tb}(z)=n_b(z)\nu_{tb}^* . \tag{8}$$

The momentum-transfer collision frequency ν_{tb} is given by Schunk.[3]

Equation (5) describes the diffusion of a minor species through a semi-infinite homogeneous background whose density $\tilde{n}_b(\tilde{z})$ is given by

$$\tilde{n}_b(\tilde{z})=\begin{cases} D & \text{for } \tilde{z}\geq 0 , \\ 0 & \text{for } \tilde{z}<0 . \end{cases} \tag{9}$$

This corresponds to the Milne problem considered by LS. With the length unit normalized as indicated in Eq. (6), the mean free path is

$$\tilde{\lambda}=1 . \tag{10}$$

In other words, we showed that the relatively general problem considered here [i.e., with a nonuniform background density $n_b(z)$] is equivalent to the much simpler Milne problem where the background density is assumed to be uniform except at $\tilde{z}=0$. Note that in earlier papers[17–18] the authors used unit lengths that are different from the one used here. For example, SB defined the mean free path (MFP) to be $(\sigma_{\text{tot}}n_b)^{-1}$, where σ_{tot} is the total collision cross section. We find it more convenient to use the new normalization factor for intercomparison of results obtained for the different study cases considered below.

III. THE MONTE CARLO METHOD

The standard procedure of the Monte Carlo technique is to follow the motion of a large number of test particles (one at a time); their positions and velocities are continually monitored. Various kinds of time averages are then computed; these averages can be equated to the corresponding ensemble averages of the system.

The simulation region of length L [in MFP units, Eq. (6)] is shown in Fig. 1. The transition between the collisionless ($\tilde{n}_b=0$) and collision-dominated media ($\tilde{n}_b\neq 0$) is at $\tilde{z}=0$. The test particles are injected into the system at $\tilde{z}=L$. Their initial velocities are generated randomly in order to be consistent with the adopted distribution function at $\tilde{z}=L+0$. The effect of a particular choice of that distribution function on the results should vanish a few mean free paths from the bottom boundary. We adopt a Maxwellian distribution which should be accurate enough for $L\gg 1$. The time interval between every two successive collisions is found via a proper random number generator. Between collisions a test particle

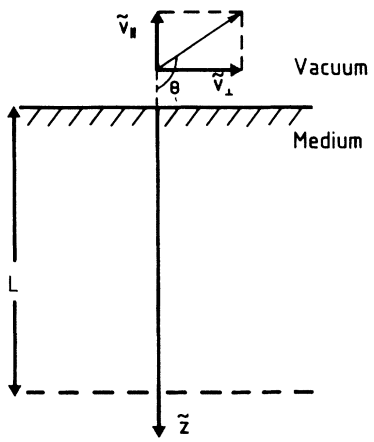

FIG. 1. Schematic representation of the model considered by the Monte Carlo method.

moves in a straight line with a constant velocity; this corresponds to neglecting the Lorentz and gravitational forces. The change of the velocity due to collisions is determined by using another set of random numbers having the statistical properties determined by the collision model.

When the test particle reaches the level $\tilde{z}=0$ with a speed that exceeds the escape velocity (v_c) it exits the simulation region; otherwise, it is reflected downward. Each test particle is tracked until it exits the system at $\tilde{z}=0$ (in this case it escapes), or at $\tilde{z}=L$; then another test particle is initiated at $\tilde{z}=L$.

The particles are monitored as they cross a predetermined set of altitudes $\{\tilde{z}_i\}$. At each altitude a suitable grid is used to register the behavior of the test particles. In this work we used two-dimensional grids whose coordinates are the velocities parallel and perpendicular to the $\tilde{z}$ axis. The symmetry in the azimuthal direction is taken into account. The time that the particles spend in each velocity bin, divided by the bin's volume, is proportional to the velocity distribution function at the bin's center. Moreover, the velocity of the particles as they cross one of the present altitudes can be directly used to find the required moments of the velocity distribution at that altitude.

A FORTRAN code (only 250 lines long) is used to implement such simulations. The results presented here are a subset of those produced by nine successful runs (1 000 000 test particles each). Typically, it takes a desktop (80 386 CPU, 20 MHz, with an 80 387-match coprocessor, AT-compatible) computer, about 35 h to implement one run.

IV. EFFECT OF MASS RATIO AND COLLISION MODEL

The procedure mentioned above is used to find the velocity distributions of the minor species at different preset altitudes. The altitude profiles of the density, drift velocity, parallel and perpendicular temperatures, parallel and perpendicular heat fluxes are obtained. These quantities are computed for different test-to-background particle mass ratios ($m_t/m_b=\frac{1}{16}$, $\frac{1}{10}$, and 1) and for different particle-interaction models (Maxwell molecule and hard-sphere interactions).

A. Maxwell molecule interaction

This interaction model is often used to simulate nonresonant ion-neutral interactions.[3] For this model the differential scattering cross section σ is independent of the scattering angle χ and inversely proportional to the relative speed g, i.e.,

$$\sigma_{tb}(g_{tb},X)=C/g_{tb} \ . \tag{11}$$

In this case the probability of collision between two (test and background) particles is independent of their velocities. We consider first the case of equal test and background masses ($m_t/m_b=1$), and zero escape velocity ($v_c=0$) which is the case of the Milne problem.

Figure 2 shows the velocity distribution function f_t at different distances from the upper boundary ($\tilde{z}=0$). At the lower boundary ($\tilde{z}=30$), the distribution function is very close to Maxwellian with a small drift velocity as it should be, by our choice. At the exobase level $\tilde{z}=1$, the distribution function shifts upward, indicating the increase in the bulk velocity as shown in Fig. 2(c). Closer to the top of the model the drift velocity increases rapidly and the velocity distribution function shows an increasing deviation from the isotropic Maxwellian distribution function. This is clearly illustrated in Fig. 2(b), for $\tilde{z}=0.1$, where the distribution function shows an asymmetry in the parallel direction with a tail in the upward direction. Note, however, that the bulk drift velocity does not coincide with the point where f_t has its maximum value.

At the top of the transition layer ($\tilde{z}=0$), all particles have velocities with upward parallel components. This feature is a consequence of the assumption that the escape velocity is equal to zero ($v_c=0$) and the absence of test particles that are injected into the system from the top.

Let us now consider the case $m_t/m_b=\frac{1}{16}$, other conditions being similar to the previous case, i.e., $v_c=0$, and Maxwell molecule model. The behavior of the distribution function for this case is quite similar to that in Fig. 2 and needs not be shown here.

The lower-order velocity moments are computed at different altitudes $\tilde{z}$. Since the Boltzmann equation is homogeneous with respect to f_t, its solution is defined within a constant factor. Therefore, the density $\tilde{n}_t$ can be normalized such that the normalized flux

$$\tilde{F}=\tilde{n}_t\tilde{u}_t=1 \ , \tag{12}$$

where the tilde is used to denote normalized quantities. The higher-order moments are normalized as follows:

$$\tilde{u}_t = \left[\frac{m_t}{2kT_b}\right]^{1/2} u_t = \left[\frac{m_t}{2kT_b}\right]^{1/2} \frac{1}{n_t} \int d\mathbf{v}_t v_{t_\parallel} f_t \ , \tag{13}$$

$$\tilde{T}_{t_\parallel} = \frac{1}{n_t}\left[\frac{m_t}{kT_b}\right] \int d\mathbf{v}_t (v_{t_\parallel} - u_t)^2 f_t \ , \tag{14}$$

$$\tilde{T}_{t_\perp} = \frac{1}{n_t}\left[\frac{m_t}{2kT_b}\right] \int d\mathbf{v}_t \, v_{t_\perp}^2 f_t \ , \tag{15}$$

$$\tilde{q}^{\,\parallel}_t = \frac{1}{n_t}\left[\frac{m_t}{2kT_b}\right]^{3/2} \int d\mathbf{v}_t (v_{t_\parallel} - u_t)^3 f_t \ , \tag{16}$$

$$\tilde{q}^{\,\perp}_t = \frac{1}{2n_t}\left[\frac{m_t}{2kT_b}\right]^{3/2} \int d\mathbf{v}_t \, v_{t_\perp}^2 (v_{t_\parallel} - u_t) f_t \ . \tag{17}$$

Figure 3 shows the distribution of the different moments for the two mass ratios ($m_t/m_b = 1$ and $\frac{1}{16}$). These profiles were found by fitting smooth curves across the points representing the values of the moments obtained by the Monte Carlo method at different altitudes. This fitting technique is used to filter out most of the residual noise which is inherent to the Monte Carlo methods. The scattering of the points about the smooth curve indicates the level of such noise. In general, the lower-order moments are very accurate; for example, the noise in the density is within the thickness of the curves shown in Fig. 3. The error increases for higher moments, especially for those with small absolute value.

The enhanced error for the higher-order moments can be explained as follows. In general, the error of the Monte Carlo method is inversely proportional to the square root of the number of particles. This noise is reflected in the irregularities seen in the tail of the distribution function (see Fig. 2). Since the higher-order moments emphasize the tail of the velocity distribution, they are expected to suffer from larger errors.

The density profiles in the two cases ($m_t/m_b = 1$ and $\frac{1}{16}$) are shown in Fig. 3(a). The difference between the two profiles is too small to show up. This near coincidence between the two curves results from the specific normalization of $\tilde{z}$, which takes the mass ratio into consideration. If we chose LS's way to normalize $\tilde{z}$, the density profiles would not have overlapped as they do here: Their slopes would be different from each other. This illustrates the advantage of the normalization method introduced here with Eq. (6). For distances far away from the vacuum-medium transition ($\tilde{z} \geq 5$) the density decreases linearly as $\tilde{z}$ decreases: $d\tilde{n}_t/d\tilde{z} = \text{const}$. But closer to the transition altitude (i.e., for $\tilde{z} \leq 1$) the density decreases faster. The linear part of the profile can be represented by the equation

$$\tilde{n}_t = m(\tilde{z} - \alpha) \ , \tag{18}$$

where m and α are constants, and α is called the extrapolation length by LS. A least-squares fit is used to find the values of m and α by fitting a straight line across the values of $\tilde{n}_t$ for $\tilde{z}$ ranging between $\tilde{z} = 5$ and $\tilde{z} = 25$. The values found for m and α are 2.008 and 0.99, respectively, for the case of $m_t/m_b = 1$, and 1.984 and 1.145, respectively, for the case of $m_t/m_b = \frac{1}{16}$.

We notice that $m \simeq 2.0$ in both cases, which can be explained using the moment equations, as shown in the Appendix. Note also that the values of m and α depend slightly on the altitude range over which the least-squares fitting has been operated.

The velocity profile is closely tied to the density profile

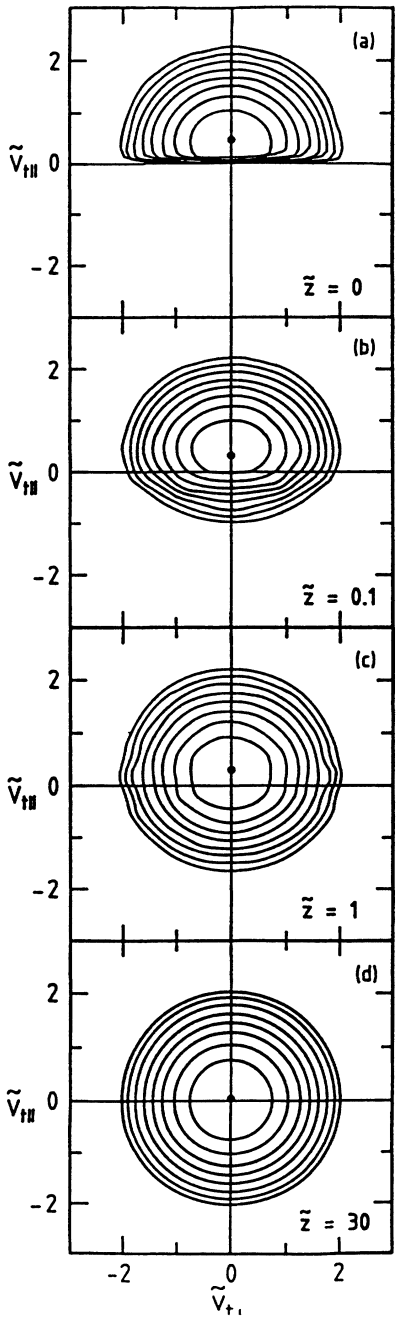

FIG. 2. Velocity distribution function f_t for the Maxwell molecule collision model, zero escape velocity ($v_c = 0$), equal masses of the test and background particles ($m_t = m_b$), and different values of the normalized distance from the transition region $\tilde{z}$ ($\tilde{z} = 0$, 0.1, 1, 30). f_t is represented by equal-value contours in the normalized velocity $(\tilde{v}_{t_\parallel}, \tilde{v}_{t_\perp})$ plane, where $\tilde{\mathbf{v}}_t = \mathbf{v}_t/(2kT_b/m_t)^{1/2}$. The contour levels decrease successively by a factor of $e^{1/2}$ from the maximum of f_t (marked by a dot).

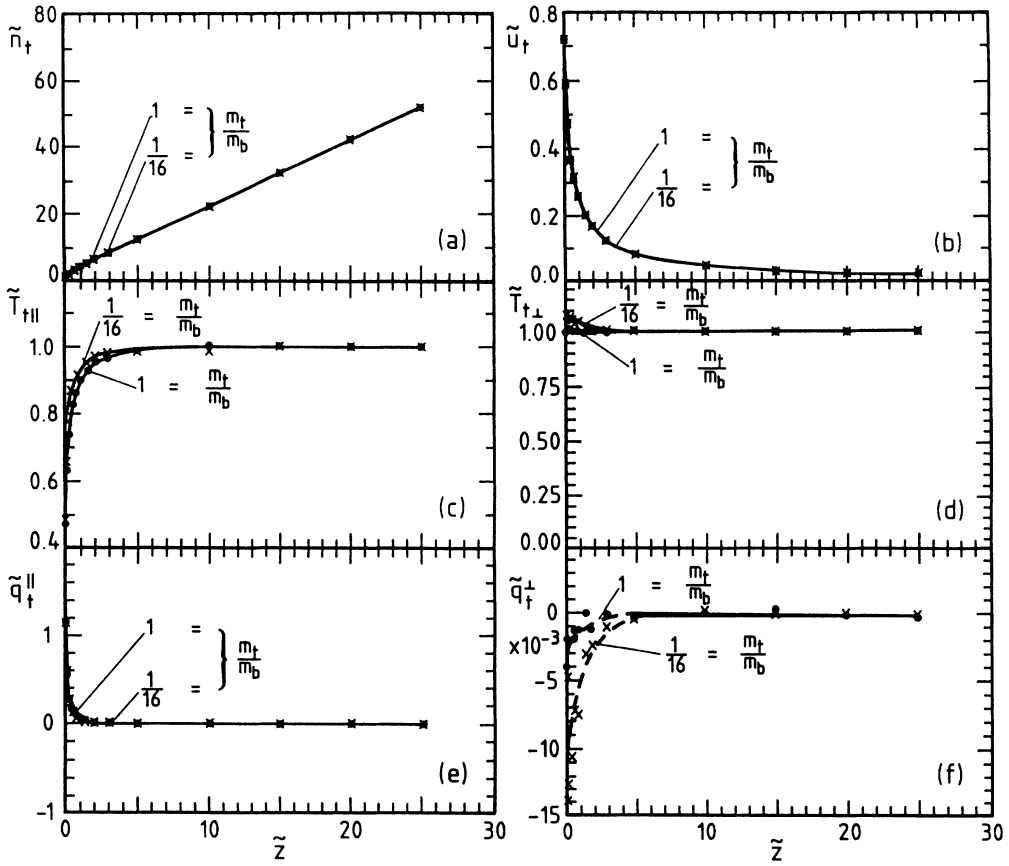

FIG. 3. Profiles of different moments of the test particles vs the normalized distance $\tilde{z}$, for a Maxwell molecule collision model, for zero escape velocity ($v_c=0$) and for two different mass ratios: $m_t/m_b=1$ and $\frac{1}{16}$. The normalized moments considered here are (a) density $\tilde{n}_t$, (b) drift velocity $\tilde{u}_t$, (c) parallel temperature $\tilde{T}_{t_\parallel}$, (d) perpendicular temperature $\tilde{T}_{t_\perp}$, (e) parallel heat flux $\tilde{q}_t^{\parallel}$, and (f) perpendicular heat flux $\tilde{q}_t^{\perp}$.

via the flux conservation relation [Eq. (12)]. Therefore, the velocity curves (for $m_t/m_b=1$ and $\frac{1}{16}$) are expected to overlap [Fig. 3(b)] as the density profiles do [Fig. 3(a)]. In fact the difference between the two profiles is larger for the region of $\tilde{z}\leq 1$ than anywhere else ($\tilde{z}\gg 1$). The test particles are very close to equilibrium for the altitudes ($\tilde{z}\gg 1$) far away from the transition level. Consequently, the bulk velocity $\tilde{u}_t$ becomes very small at $\tilde{z}\gg 1$. As $\tilde{z}$ decreases the test species deviates more and more from equilibrium due to the missing particles, because they escaped at $\tilde{z}=0$. For a smaller value of $\tilde{z}$, the importance of the escaping particle increases, and consequently $\tilde{u}_t$ increases rapidly as $\tilde{z}\to 0$.

Figure 3(c) shows the profiles of the parallel temperature $\tilde{T}_{t_\parallel}$. The minor species retains an equilibrium temperature equal to that of the background ($\tilde{T}_{t_\parallel}=T_{t_\parallel}/T_b\simeq 1$) in the region $\tilde{z}\gg 1$. For $\tilde{z}\leq 1$, the distribution function misses a large percentage of the downgoing particles owing to their escape. This results in an increase of the parallel drift energy ($\tilde{u}_t^2$) at the expense of the parallel thermal energy ($\tilde{T}_{t_\parallel}$). This accounts for the sharp decrease in $\tilde{T}_{t_\parallel}$ in this region, until it becomes approximately equal to 0.4 at $\tilde{z}=0$. Note that in the region $\tilde{z}\lesssim 5$ the two profiles are slightly different, with $\tilde{T}_{t_\parallel}$ higher for the case of $m_t/m_b=\frac{1}{16}$. This may be attributed to the larger coupling between the coherent and the random energies[3] when the mass ratio m_t/m_b is smaller.

The perpendicular temperature $\tilde{T}_{t_\perp}$ [Fig. 3(d)] retains its equilibrium value over a wide range of altitudes, except for a slight increase near $\tilde{z}=0$. This increase is due to the drift and thermal energy coupling. As mentioned above this coupling is higher for the case of $m_t/m_b=\frac{1}{16}$, and consequently the increase in $\tilde{T}_{t_\perp}$ is higher for this case.

As shown in Fig. 3(e), the parallel heat flow $q_t^{\parallel}$ stays close to zero until $\tilde{z}\simeq 1$, where it increases very rapidly to attain a value greater than 1 for $\tilde{z}=0$ ($\tilde{q}_t^{\parallel}=1.28$ and 1.18 for $m_t/m_b=1.0$ and $\frac{1}{16}$, respectively). This large (positive) value is associated with the asymmetry (with an upward tail) that develops in the distribution function near $\tilde{z}=0$.

The perpendicular heat flow $\tilde{q}_t^{\perp}$ is very small everywhere [Fig. 3(f)] although it shows a tendency to become negative as $\tilde{z}\to 0$, with $\tilde{q}_t^{\perp}$ more negative for the case of $m_t/m_b=\frac{1}{16}$ than for $m_t/m_b=1$. The curves are dashed

near the top (for $\tilde{z} \leq 4$) because of the large noise inherent in the MC method when $q_t^{\perp}$ is computed.

B. Hard-sphere interaction

For the hard-sphere collision model (HS) the differential scattering cross section σ_{tb} is independent of both the scattering angle χ and the relative speed g_{tb}:

$$\sigma_{tb}(g_{tb},\chi)=C' , \tag{19}$$

where C' is a constant determined by the radii of the colliding particles. This model is adequate to describe elastic collision between neutral atoms. Since the probability of collision between two particles (for the HS model) is dependent on their relative velocity, we used the "null collision" technique in order to randomly generate the time intervals between successive collisions. This technique is explained in detail by Lin and Bardsley.[24]

The general characteristics of the velocity distribution function f_t for the hard-sphere model is quite similar to that for the Maxwell molecule collision model shown in Fig. 2 and not displayed here. On the other hand, the moments of the velocity distribution function for the HS case (Fig. 4) show few, yet physically significant, differences in comparison with the Maxwell molecule (MM) case (Fig. 3).

(1) Use of Eq. (18) and a least-squares fit to the linear part of the density profile results in $\alpha=1.028$ and $m=1.95$ for the case of $m_t/m_b=1$, and $\alpha=0.998$ and $m=1.81$ for the case of $m_t/m_b=\frac{1}{16}$. This shows that for the HS collision model the density gradient depends on the mass ratio m_t/m_b and is different from the constant value it assumes ($m=2$) for the MM collision model. This is due to the heat-flow correction to the diffusion coefficient [see Eq. (A3)], which is absent for the MM collision model and depends on the target-to-background particle mass ratio m_t/m_b for the other collision models (including the HS one).

(2) Similarly, there is a noticeable deviation between the velocity profiles for the two mass ratios ($m_t/m_b=1$ and $\frac{1}{16}$), in contrast to the case of the MM model, where the velocity profiles showed very little dependence on the mass ratio m_t/m_b.

(3) The perpendicular temperature $\tilde{T}_{t_\perp}$ decreases slightly as $\tilde{z}\rightarrow 0$. This can be understood in the light of the following argument. Consider two particles (1 and 2) starting from the same altitude with the same upward parallel velocity component. Particle 1 has a larger perpendicular velocity component than that of particle 2. The collision frequency increases with $|v|$ for the HS model. Therefore, compared to particle 1, particle 2 has a greater chance to reach a higher altitude before it is scattered downward. That is, the collisions work as a filter that

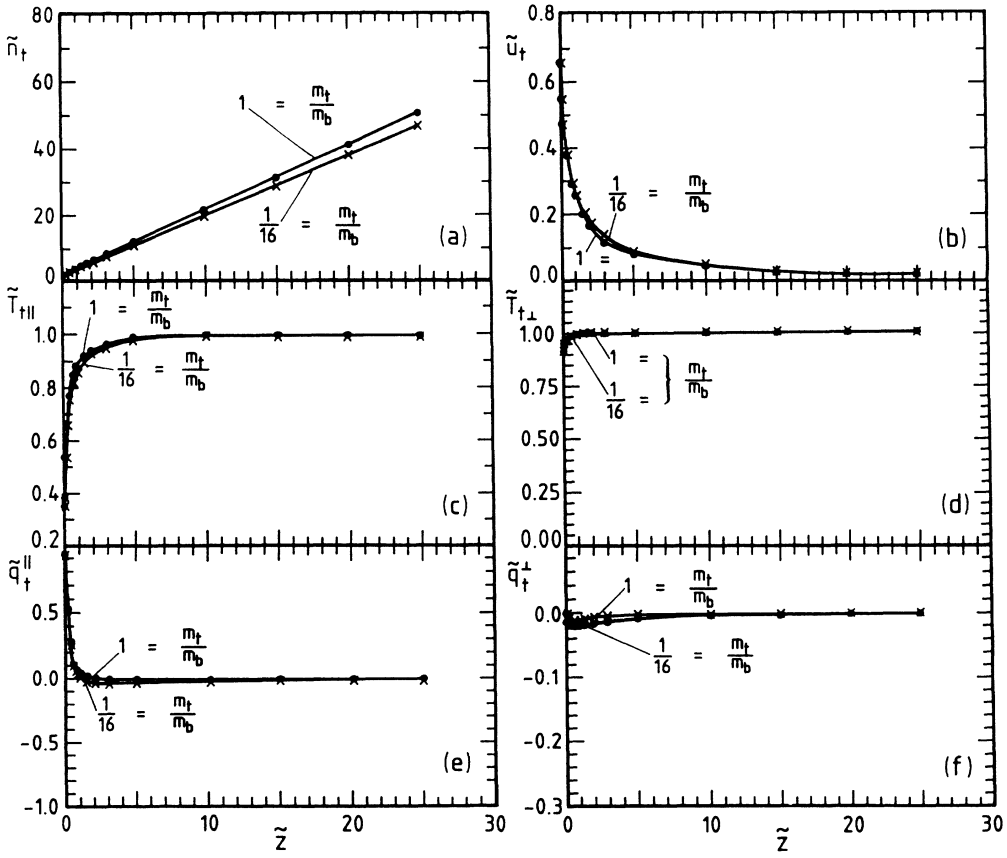

FIG. 4. Profiles of different moments of the test particles vs the normalized distance $\tilde{z}$, for a hard-sphere collision model, for zero escape velocity ($v_c=0$), and for two different mass ratios: $m_t/m_b=1$ and $\frac{1}{16}$. The format is similar to that in Fig. 3.

reflects more particles with large perpendicular energy and permits more particles with small perpendicular energy to pass. This explains why the region $\tilde{z} \leq 1$ is more accessible to particles with smaller perpendicular energies, and, consequently, the perpendicular energy $\tilde{T}_{t_\perp}$ decreases in this region.

(4) The parallel heat flow $\tilde{q}_t^{\parallel}$ is negative for $\tilde{z} \geq 2$. As we approach the region $\tilde{z} \leq 1$, $\tilde{q}_t^{\parallel}$ becomes positive very rapidly and reaches a value $\simeq 1$ at $\tilde{z}=0$. The perpendicular heat flow $\tilde{q}_t^{\perp}$ remains negative at all altitudes. It reaches a minimum at $\tilde{z} \sim 1$, and vanishes at $\tilde{z}=0$. The behavior of $\tilde{q}_t^{\perp}$ can be explained using the idea of the "perpendicular energy filter" mentioned earlier. In the region $\tilde{z} \sim 1$ the down-going (reflected) particles have larger perpendicular energy than the up-going ones. This results in negative values for $\tilde{q}_t^{\perp}$. At $\tilde{z}=0$ all the particles are moving in the upward direction. Since no collision (filter) occurs above that point, the heat flow $\tilde{q}_t^{\perp}$ returns to zero.

V. COMPARISON WITH PREVIOUS MONTE CARLO STUDIES

Chamberlain and Campbell[22] studied the rate of evaporation of a non-Maxwellian atmosphere. They used a Monte Carlo algorithm, and a hard-sphere collision model, in order to study the escape of H and He in an oxygen background. Later, some inaccuracies were discovered and corrected by the authors in a subsequent work.[23] They computed the escape fluxed for different values of background temperatures (T_b). They found that the actual-to-Jeans escape-flux ratio $F/F_J \sim 0.7$ for H and ~ 0.92 for He. They also found that $F/F_J \sim 0.55$ for H in a CO_2 atmosphere.[25] (See Table I, for definition of the Jeans escape flux F_J.)

These results were confirmed by an independent algorithm by Brinkmann.[20,21] This latter code incorporated a more realistic interparticle collision model. It also used the concept of "virtual particles" in order to improve the code's efficiency. These codes share many features with ours because all of them are based on MC algorithms. However, there are some characteristics that distinguish our algorithm from the others, such as the following.

(i) We incorporated the "null collision" concept, which simplified the code, and reduced the storage space. This also makes it easier to include the gravitational and Lorentz forces on the particle motion between collisions (if needed in future work).

(ii) We avoided using complicated algorithms such as the auditing algorithm used by Chamberlain and Smith,[22,23] and the algorithm that assigns initial velocity for the test particles used by Brinkmann.[20]

(iii) We did not use the "virtual particle" concept, which, however, may be worth including in the future.

Items (i) and (ii) result in a greater simplification in the algorithm which makes it easier to code, debug, maintain, and modify at the expense of more CPU time.

The corrected results of the previous works were mainly concerned with the escape flux of light atoms from planetary atmosphere. Although our work is not intended to address this problem in detail, for completeness we compare our values of F/F_J to the relevant values predicted by the other computations. Table I compares the results of (i) the previous MC codes, (ii) the QDM methods, and (iii) this work. However, different definitions of Jeans flux were used for the MC (Ref. 20) and the QDM method (see Table I). Therefore, we present our results using both definitions for the Jeans flux (last two columns of Table I). Table I shows that our results are in good agreement with the other works, especially when one considers the following.

(i) The values of F/F_J and F/F_J^* in the present work tend to bracket the results of the MC and the QDM.

(ii) Our code was not directly designed to produce particularly accurate values of escape fluxes [had this been our intention, some variance-reduction techniques (e.g., virtual particles[20]) could have been used instead].

(iii) The actual differences existing between the calculated flux F computed with the QDM and previous MC (Ref. 23) methods are larger than may appear from Table I, owing to the fact that the Jeans Fluxes F_J and F_J^* were defined differently in these references.

TABLE I. Comparison of the values of the escape flux (normalized to the Jeans flux) with those computed in previous works. $F_J = n_c(kT_b/2\pi m_t)^{1/2}(1+\lambda)\exp(-\lambda)$, where $\lambda = m_t v_c^2/2kT_b$; $F_J^* = n_c(kT_{tc}/2\pi m_t)^{1/2}(1+\lambda_c)\exp(-\lambda_c)$, where $\lambda_c = m_t v_c^2/2kT_{tc}$. Subscript c indicates values at 1 MFP. From the top.

		Previous MC[a]	QDM[b]	Present work	
$\frac{v_c}{\sqrt{2kT_b/m_t}}$	T_b	F/F_J	F/F_J^*	F/F_J	F/F_J^*
3	780			0.72	0.75
2.5	1100	0.725	0.75		
2.15	1500	0.680	0.70		
2.0	1750		0.69	0.63	0.78
1.6	2700	0.670	0.66		
1.4	3570	0.669	0.65		

[a]Reference 23.
[b]Reference 1.

VI. COMPARISON WITH DIRECT SOLUTIONS OF THE BOLTZMANN EQUATION

There have been several attempts to solve special cases of the problem considered above, by directly solving the Boltzmann equation. For example, LS solved the Milne problem for a hard-sphere collision model and for zero escape velocity ($v_c=0$). They considered a general solution as a sum of spatial transient and asymptotic functions, which, in turn, were expanded in Burnett functions. SB used the discrete ordinate method (QDM) to solve the Boltzmann equation, and hence study the departure from equilibrium in the exosphere of a planet due to the loss of thermal hot atoms. A nonzero escape velocity was used by SB to simulate the effect of gravity. In this section we will compare the results of the works mentioned above to those of the Monte Carlo method.

A. Zero escape velocity

In order to compare the Monte Carlo results with those of LS, we considered the case of zero escape velocity, the hard-sphere collision model, and different mass ratios m_t/m_b.

First, we consider the calculation of the "extrapolation length" α, which corresponds to the point where the asymptotic density-profile equation (18) becomes equal to zero. Figure 5 represents the extrapolation length α for different mass ratios m_t/m_b. The two lines correspond to the results of LS for different approaches of applying the boundary conditions. Note that the extrapolation length was renormalized to be consistent with Eq. (6). We notice that α remains very close to unity for all values of the mass ratio. Moreover, the singularity of α for $m_t/m_b \rightarrow \infty$ that LS refer to, disappears as a result of the new normalization used here. This supports even further that the definition of the mean free path, used to normalize z in this paper, is of great practical interest [Eqs. (6) and (10)].

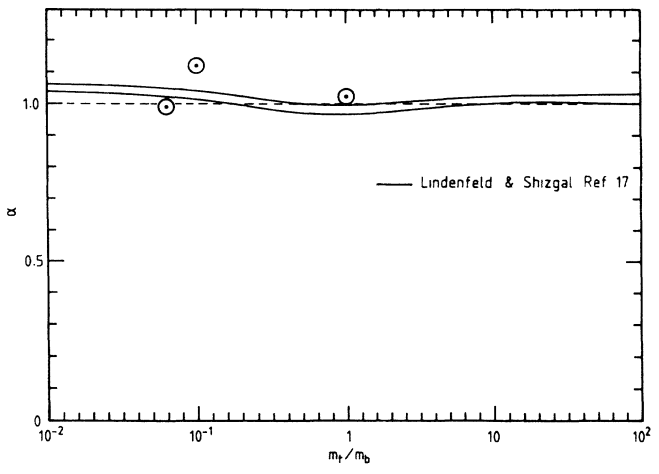

FIG. 5. Comparison between the Monte Carlo normalized extrapolation length α, and that found by direct solution of the Boltzmann equation (LS). α is plotted vs the test-to-background mass ratio m_t/m_b. The Monte Carlo results are represented by the encircled dots, while the solid lines represent the results of LS for two different approaches in handling the boundary conditions. Zero escape velocity ($v_c=0$), and a hard-sphere collision model are considered.

The circled dots represent the values of α computed by the Monte Carlo methods for $m_t/m_b=1$, $\frac{1}{16}$, and $\frac{1}{10}$. We notice that the Monte Carlo results are quite acceptable, compared to the difference between the two curves which may be used as a measure of the uncertainty in the direct solution method. It is worth pointing out that, although the densities predicted by the MC method are rather accurate, the values of α suffer from larger uncertainties ($\sim 5\%$). This is because α is computed via a mathematical procedure that involves the subtraction of two numbers that have nearly equal magnitudes and opposite signs, which significantly increases the uncertainty in the result.

The azimuthal variation of the test particle distribution function for constant velocity ($v_t=$const) at $\tilde{z}=0$ is presented here to facilitate the comparison with LS. Figure 6 shows the normalized distribution function versus $\cos(\theta)$, where θ is the angle between $\mathbf{v}_t$ and the $\tilde{z}$ axis (Fig. 1). Two mass ratios ($m_t/m_b=1$ and 0.1) and four normalized velocities ($\tilde{v}_t=v_t/\sqrt{2kT_b/m_t}$) are considered. The points (+ for $m_t/m_b=1$ and $\times$ for $m_t/m_b=0.1$) are the Monte Carlo results to which the solid lines are fitted. The agreement between the points and the fitted lines may be considered as a measure of the accuracy of the Monte Carlo results. We notice that the results are quite accurate, except in the tail of the distribution function (e.g., $\tilde{v}_t=2$) especially for velocities that are almost parallel to the z axis ($\cos\theta=\pm 1$). The problem of accuracy for $\cos\theta=\pm 1$ is a consequence of the specific binning grid used here (the bin size is indeed proportional to $v_{t_\perp}$). This results in smaller bin sizes (and consequently larger relative error) for $v_{t_\perp}\simeq 0$ (i.e., $\cos\theta\simeq\pm 1$). This problem may, however, be eliminated using a different binning scheme. On the contrary, the inaccuracy of the Monte Carlo results in the tail of the distribution function is more inherent to this method and can only be reduced by increasing the number of test particles. The relative error is proportional to $N^{-1/2}$ (N is the number of particles per bin), and therefore increases rapidly in the tail of the velocity distribution, where $N\rightarrow 0$.

We notice from Fig. 6 that the distribution function is peaked in the forward direction, and decreases more rapidly as $\cos\theta$ increases. It becomes zero for $\cos\theta\geq 0$, as expected from the boundary conditions. For $\tilde{v}_t=0.4$ (top), the distribution function is more peaked for $m_t/m_b=0.1$ than it is for $m_t/m_b=1$. As $\tilde{v}_t$ increases, this difference decreases and eventually reverses, as shown for $\tilde{v}_t=2$ (bottom). These features are consistent with the results of LS.

The method used by LS uses a finite number of polynomials to approximate the distribution function. Oscillations of f_t versus $\cos\theta$ are a direct consequence of this approximation. These oscillations result in nonphysical results ($f_t<0$) for certain ranges of θ. In comparison, the Monte Carlo method does not suffer from this type of

deficiency. However, the Monte Carlo method gives results only at discrete points, while the other method gives continuous solutions.

B. Nonzero escape velocity

So far, we have considered only cases with zero escape velocity (i.e., the Milne problem); we now consider the cases of nonzero escape velocities which are more relevant to the exospheric escape of atoms from a planetary atmosphere. The physical conditions are chosen in order to facilitate comparison with the work of SB. In SB, the quadrature discretization method was used to solve the Boltzmann equation for the escape of light atoms through a heavier major constituent (say H in O). In particular, we consider $m_t/m_b=\frac{1}{16}$, and the hard-sphere collision model.

The ratio of the escape flux F and the Jeans escape flux F_J are shown in Table I. The agreement of these values and SB's results was discussed earlier.

Figure 7 shows the density profiles for different escape velocities. For presentation purposes, the densities are arbitrarily renormalized such that the density at $\tilde{z}=3$ is unity in all cases. For the case of $\tilde{v}_c=0$, already discussed above, the density decreases linearly at $z\gg 1$, then the density gradient becomes steeper at $\tilde{z}\leq 1$. As the escape velocity $\tilde{v}_c$ increases, more particles are reflected. This results in a reduction of the escape flux and consequently a reduction of the density gradient as $\tilde{v}_c$ increases. For a very high escape velocity ($\tilde{v}_c\geq 3$), very few particles escape, and the density gradient becomes too small to be detected with the Monte Carlo method. These results are consistent with the corresponding ones in SB.

We notice that the features associated with a lower boundary (e.g., the larger density gradient and elevated temperature) in the results of SB do not appear in the Monte Carlo results: This is due to the larger model length L in the latter case (i.e., in the MC simulation). In SB, the authors suggested that the temperature overshoot might be real, but cautioned that this region was poorely sampled, i.e., that there were few quadrature points in this region. Such unexpected features may be attributed to a lack of consistency in the lower-boundary conditions. Indeed, they disappear within a few mean free paths from

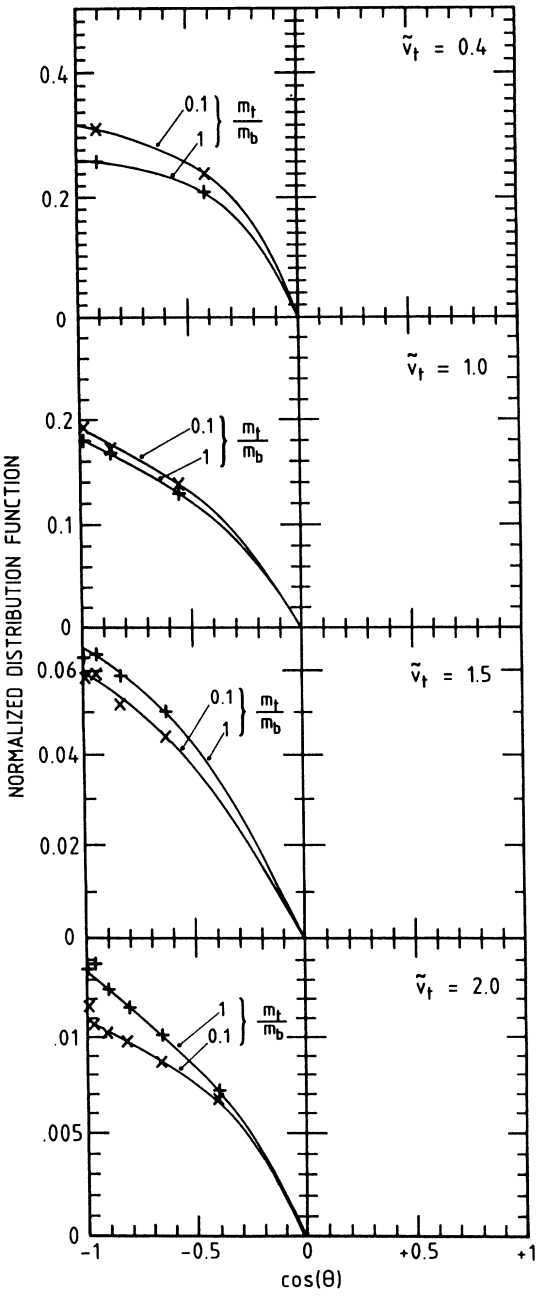

FIG. 6. Normalized test particle distribution function vs $\cos(\theta)$ for constant v_t, at the transition region ($\tilde{z}=0$). Two different mass ratios ($m_t/m_b=1$ and 0.1) and four values of the normalized test particle velocities are considered ($\tilde{v}_t=v_t/\sqrt{2kT_b/m_t}=0.4$, 1, 1.5, and 2, from top to bottom). Zero escape velocity ($v_c=0$) and a hard-sphere collision model are considered.

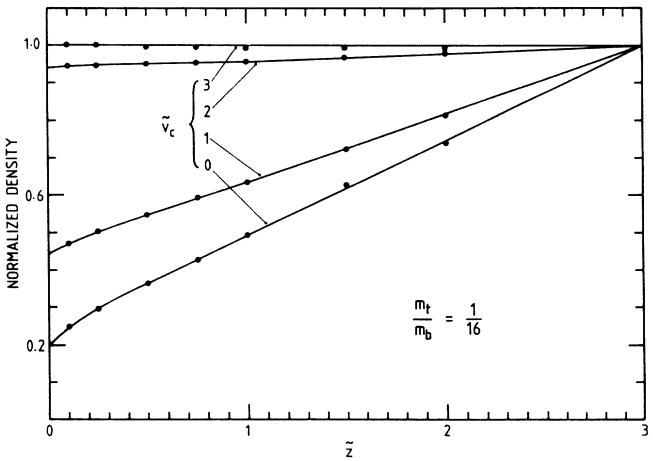

FIG. 7. Test particle density profiles for different values of normalized escape velocity ($\tilde{v}_c=v_c/\sqrt{2kT_b/m_t}=0$, 1, 2, and 3). The densities are arbitrarily renormalized to equal unity at $\tilde{z}=3$. A mass ratio ($m_t/m_b=\frac{1}{16}$) and a hard-sphere collision model are considered.

the lower boundary. No special feature should appear near the lower boundary of the model.

VII. COMPARISON WITH THE SOLUTION OF THE MOMENT EQUATIONS

Instead of the kinetic approaches of LS and SB, it is possible to replace the Boltzmann equation by a hierarchy of transport equations for the different velocity moments of the distribution function (such as density, momentum, energy, etc.). This infinite set of equations is then truncated at a convenient level using physical or mathematical arguments. In the rest of this section we will be concerned with 13-moment equations. This hydrodynamical approximation is obtained by expanding the distribution function about a drifting Maxwellian. A detailed description of this set and its properties is given by Schunk[3] and shall not be repeated here. The comparison between the 13-moment equations and the Monte Carlo method will be addressed in a future work. Here, we will only make the following remarks.

(i) The moment equations can only retain a finite number of moments,[3] while the Monte Carlo method solves for the distribution function which is, in principle, equivalent to retaining all the moments. The Monte Carlo result may be used to check the validity of the solution of the moment equations.

(ii) A major advantage of the moment-equations method is its ability to handle large-scale models.[6-8] It can be used (in the regions where it is valid) to complement the Monte Carlo method that is useful to small scale models (few tens of mean free paths).

(iii) The Monte Carlo model is very useful in solving for the stationary trans-sonic flow where the moment equations generally have mathematically singularities.[26]

(iv) The moment equations can be used to improve the accuracy of the high-order moments computed by the Monte Carlo, for $\tilde{z} \gg 1$, and to extrapolate the results beyond the range of distance where the Monte Carlo model is defined (see the Appendix).

VIII. SUMMARY AND CONCLUSION

The Monte Carlo method is a technique that can be used to solve the Boltzmann equation by particle simulations. In spite of its attractive features, its practicality is primarily dependent on the availability of computing resources. The MC technique is now a very accepted methodology in a large number of problems in science and engineering.

In recent years, powerful desktop computers became available at reasonable prices. This trend, which is expected to continue in the future, resulted in an underutilization of a significant amount of the computing power (especially desktop computers) available to the scientific community. The Monte Carlo (one-particle) simulations, such as that considered here, are good candidates to utilize this CPU power that otherwise would be wasted. They are especially suited to run on personal computers for the following reasons.

(i) Their codes are simple and short, which does not tax the limited resources of a PC.

(ii) They do not require large arrays, and therefore can fit easily in the PC's relatively small memory.

(iii) More than one computer (or processor) can be used simultaneously to solve the same problem. Each computer can perform the simulation for a different set of random numbers. The results can then be combined to produce the final answer.

We considered the problem of the escape of a minor species through a major species for different mass ratios ($m_t/m_b = 1, \frac{1}{10}, \frac{1}{16}$). The gravitational force was simulated by a barrier that reflects particles that reach the upper boundary with an up-going velocity larger than an escape velocity v_c. Different collision models (Maxwell molecule and hard sphere) and different values of v_c were considered. A Monte Carlo simulation was used to compute the minor-species distribution function f_t, density $\tilde{n}_t$, drift velocity $\tilde{u}_t$, parallel and perpendicular temperatures ($\tilde{T}_{t_\parallel}, \tilde{T}_{t_\perp}$), and parallel and perpendicular heat fluxes ($\tilde{q}_t^{\parallel}, \tilde{q}_t^{\perp}$). A small subset of all the results obtained was presented above. This subset was chosen to illustrate the behavior of the minor species for different physical conditions, and to facilitate comparison with the alternative methods like the kinetic and hydrodynamic approaches of solving the same problem. The following results were found.

(i) $\tilde{v}_c = 0$. First for $v_c = 0$ we found the following.

(a) For both of the hard-sphere and Maxwell molecule interaction models, the distribution is very close to a drifting Maxwellian (with $\tilde{T}_t \simeq 1$) at distances far from the transition region. As one approaches the transition region the bulk velocity increases and anisotropy ($\tilde{T}_{t_\parallel} < \tilde{T}_{t_\perp}$) as well as an asymmetry with an upward tail for f_t develops at a few mean free paths from the top of the diffusion medium.

(b) For both collision models, the drift velocity $\tilde{u}_t$ increases slowly at first, and then more rapidly as $\tilde{z}$ decreases.

(c) For both models, the parallel temperature $\tilde{T}_{t_\parallel}$ decreases below its equilibrium value (1), and the parallel heat flow $\tilde{q}_t^{\parallel}$ attains large positive values at $z \leq 1$.

(d) As $\tilde{z} \to 0$, the perpendicular temperature $\tilde{T}_{t_\perp}$ increases slightly for the Maxwell molecule collision model while it shows a slight decrease for the hard-sphere model.

(e) For the Maxwell molecule model, the density gradient, $d\tilde{n}_t/d\tilde{z}$, equals 2 (at $\tilde{z} \gg 1$), as predicted by the momentum equations; this density gradient is independent of the test-to-background particle mass ratio (m_t/m_b).

(f) In contrast, for the case of the hard-sphere model, $d\tilde{n}_t/d\tilde{z}$ is less than 2 (at $\tilde{z} \gg 1$) and depends on the mass ratio (m_t/m_b). This is due to the mass-dependent heat-flow term in the momentum equation.

(ii) $v_c \neq 0$. Second, as v_c increases, less particles are able to escape at the top boundary, and consequently the relative density gradient $d\ln(\tilde{n}_t)/d\tilde{z}$ decreases. The change in the density becomes smaller than the uncertainty in the Monte Carlo results, for $\tilde{v}_c \geq 3$.

The Monte Carlo results were compared to those obtained by direct solution of the Boltzmann equation, either by expansion in Burnett functions (LS), or by a quadrature discretization method (SB) (kinetic solutions). The Monte Carlo solutions were found to be consistent with the results of these kinetic solutions. However, the following differences between the two approaches can be pointed out.

(a) Because of the limited number of terms taken into account in the polynomial expansion of the solution of Boltzmann's equation, spurious oscillations in the $[f_t, \cos(\theta)]$ relation are produced, especially near $\tilde{z}=0$; these mathematical artifacts can be reduced by increasing the number of terms in the expansion series, in the same way as the large errors obtained with the MC method for the higher-order moments can be reduced by increasing the number of test particles. Nevertheless, such numerical oscillations do not exist for the Monte Carlo results.

(b) The Monte Carlo method is mathematically less involved, and requires simpler computer programming compared to the kinetic or hydrodynamic approaches.

(c) The Monte Carlo algorithm can be adapted easily to handle other physical situations (e.g., other collision models, more than one background species, external forces, etc.). In contrast, it is difficult, if not impossible, to adapt the other method to other situations without rewriting a new numerical code.

(d) The Monte Carlo results are given at a discrete set of values, and an interpolation technique should be used to find the results at other points. Note that a similar procedure can be used in the quadrature discretization method to smooth the oscillations of the numerical solutions mentioned above as a drawback of this otherwise powerful and elegant method.

(e) The Monte Carlo results suffer from a poor precision (typically two significant digits) in contrast to the other nonstatistical methods.

(f) The accuracy of the Monte Carlo results decreases as the number of particles per bin decreases. This makes it less reliable for the tail of the distribution function, and for quantities that are functions of many independent variables (>2).

In comparison to the hydrodynamic or moment equations, the Monte Carlo method showed some advantages, but also some limitations. The two approaches may be used judiciously in order to complement each other. Further investigations in this direction are promising.

As the Monte Carlo technique becomes more frequently used, attention should be paid to improving some of the less refined codes that are in circulation. For example, identifying the better algorithms that generates sequences of pseudorandom numbers; systematically testing the statistical properties of the pseudorandom number sequences[27] before using them in the simulation; using algorithms that systematically estimate the uncertainties of the solutions; using techniques of filtering out the random noise in the results, in order to improve their accuracy; and using the existing "variance-reduction" techniques, and developing new ones in order to improve the reliability of the results.

APPENDIX

In the case of the Milne problem ($v_c=0$), for the Maxwell molecule and under the conditions $\tilde{z}\gg 1$, the 13-moment equations become

$$\frac{d\tilde{n}_t}{d\tilde{z}}=2\ , \tag{A1}$$

$$\tilde{q}_t=-\tfrac{5}{4}(1/D_{tb}^{(1)})\tilde{u}_t\ , \tag{A2}$$

where $D_{tb}^{(1)}$ is given by Schunk.[3] The solution of Eq. (A1), is the linear density profile given in Eq. (18) with $m=2$.

From Eqs. (12), (18), and (A2) we find that in the collision-dominated region ($\tilde{z}\gg 1$) the heat flux is

$$\tilde{q}_t=-\frac{\frac{5}{8}}{D_{tb}^{(1)}(\tilde{z}-\alpha)}\ , \tag{A3}$$

which gives more accurate values than those of the Monte Carlo method in the region $1\ll\tilde{z}\le L$ and remains valid outside the MC modeling region (i.e., for $\tilde{z}>L$).

If we follow an argument similar to that mentioned above, we can get similar relations corresponding to other collision models. For the hard-sphere collision model, starting from the 13-moment equations with Burgers linear collision terms,[3] we then obtain

$$\frac{d\tilde{n}_t}{d\tilde{z}}=2\left[1+\frac{5}{2}\frac{Z_{tb}}{D_{tb}^{(1)}}\frac{m_b}{m_t+m_b}\left[1-\frac{m_bZ_{tb}}{m_t+m_b}\right]\right]\ , \tag{A4}$$

where Z_{tb} is a dimensionless quantity defined in Schunk.[3]

---

*On leave from Utah State University, Logan, UT 84322.

[1]B. Shizgal and R. Blackmore, Planet. Space Sci. **34**, 279 (1986).
[2]B. Davison, *Neutron Transport Theory* (Oxford University Press, Oxford, 1957).
[3]R. W. Schunk, Rev. Geophys. Space. Sci. **15**, 429 (1977).
[4]P. M. Banks and T. E. Holzer, J. Geophys. Res. **73**, 6846 (1968).
[5]P. M. Banks and T. E. Holzer, J. Geophys. Res. **74**, 6317 (1969).
[6]R. W. Schunk and D. S. Watkins, J. Geophys. Res. **86**, 91 (1981).
[7]R. W. Schunk and D. S. Watkins, Geophys. Res. **87**, 171 (1982).
[8]H. G. Demars and R. W. Schunk J. Geophys. Res. **92**, 5969 (1987).
[9]J. Lemaire and M. Scherer, Planet. Space Sci. **18**, 103 (1970).
[10]J. Lemaire and M. Scherer, Rev. Geophys. **11**, 427 (1973).
[11]T. E. Holzer, J. A. Fedder, and P. M. Banks, J. Geophys. Res. **76**, 2453 (1971).
[12]A. R. Barakat and R. W. Schunk, J. Geophys. Res. **88**, 7887 (1983).
[13]A. R. Barakat and R. W. Schunk, J. Geophys. Res. **89**, 9771 (1984).
[14]J. Lemaire, J. Atmos. Terr. Phys. **34**, 1647 (1972).

[15]H. J. Fahr and B. Shizgal, Rev. Geophys. Space Phys. **21**, 75 (1983).
[16]B. Shizgal, U. Weinert, and J. Lemaire, in *Proceedings of Rarefied Gas Dynamics 26,* edited by V. Boffi and C. Cercignami (Teubner, Stuttgart, 1986), pp. 374–383.
[17]M. J. Lindenfeld and B. Shizgal, Phys. Rev. A **27**, 1657 (1983).
[18]B. Shizgal and R. Blackmore, J. Comput. Phys. **55**, 313 (1984).
[19]G. H. Wannier, Bell Syst. Tech. J. **32**, 170 (1953).
[20]R. T. Brinkman, Planet. Space. Sci. **18**, 449 (1970).
[21]R. T. Brinkman, Planet. Space Sci. **19**, 791 (1971).
[22]J. A. Chamberlain and F. J. Campbell, Astrophys. J. **149**, 687 (1967).
[23]J. W. Chamberlain and G. R. Smith, Planet Space Sci. **19**, 675 (1971).
[24]S. L. Lin and J. N. Bardsley, J. Chem. Phys. **66**, 435 (1977).
[25]J. W. Chamberlain, Astrophys. J. **155**, 711 (1969).
[26]R. W. Schunk (private communication).
[27]D. E. Knuth, *The Art of Computer Programming, Vol. 2: Seminumerical Algorithms* (Addison-Wesley, London, 1981).